

# Synthesis, characterization, and crystal structures of 2D cobalt(II) and nickel(II) coordination polymers containing flexible bis(benzimidazole) ligands

Jing Wang Cui<sup>1</sup> · Yong Guang Liu<sup>1</sup> · Zeng Chuan Hao<sup>1</sup> · Gui Ying Dong<sup>1</sup>

Received: 25 January 2016 / Accepted: 14 March 2016  
© Springer International Publishing Switzerland 2016

**Abstract** Three coordination polymers, namely  $\{[\text{Ni}(\text{L1})(\text{nip})(\text{H}_2\text{O})]\cdot 2\text{H}_2\text{O}\}_n$  (**1**),  $[\text{Co}(\text{L2})(\text{tbip})]_n$  (**2**), and  $\{[\text{Co}_2(\text{L3})_2(\text{bptc})]\cdot 3\text{H}_2\text{O}\}_n$  (**3**) (L1 = 1,4-bis(5,6-dimethylbenzimidazole)butane, L2 = 1,4-bis(5,6-dimethylbenzimidazole)-2-butylene, L3 = 1,3-bis(5,6-dimethylbenzimidazole)propane, H<sub>2</sub>nip = 5-nitro-isophthalic acid, H<sub>2</sub>tbip = 5-tert-butyl-isophthalic acid, H<sub>4</sub>bptc = biphenyl-3,3',4,4'-tetracarboxylic acid), have been synthesized under hydrothermal conditions and characterized by physicochemical and spectroscopic methods as well as by single-crystal X-ray diffraction analysis. Complexes **1** and **2** both feature a two-dimensional (4,4) layer with (4<sup>4</sup> × 6<sup>2</sup>) topology. Complex **3** possesses a uninodal 4-connected 2D **htb** network. The fluorescence spectra and catalytic properties of the complexes for the degradation of methyl orange by sodium persulfate in a Fenton-like process are reported.

## Introduction

The design and synthesis of coordination polymers (CPs) are currently attracting much attention, due to their intriguing topologies and potential applications in

absorption, catalysis, luminescence, and magnetism [1–5]. However, it is still difficult to rationally construct CPs with specific structures and properties. Many factors, such as the choice of organic linkers, metal, solvent, reaction temperatures, and reaction pH value, may significantly influence the structures of the resulting CPs [6–8]. Among these factors, an important key to assemble CPs is the proper selection of organic bridging ligands [9, 10]. As excellent multifunctional ligands, aromatic carboxylic acids offer both versatile coordination modes and high structural stability [11–13]. For example, 5-nitro-isophthalic acid (H<sub>2</sub>nip), 5-tert-butyl-isophthalic acid (H<sub>2</sub>tbip), and biphenyl-3,3',4,4'-tetracarboxylic acid (H<sub>4</sub>bptc) have been used extensively in the synthetic strategies to develop multidimensional (zero, one, two, and three dimensional) complexes [14, 15]. Meanwhile, flexible bis(benzimidazole)s are versatile ligands that can meet the coordination requirements of the metal centers by means of their variable conformations [16, 17]. Furthermore, methyl substituent groups can be used to enhance the electron-donating ability of these bis(benzimidazole) derivatives [18–20]. Herein, a mixed-ligand synthetic strategy has been applied to prepare transition metal CPs by the judicious selection of neutral N-donor ligands and aromatic carboxylates. In this way, three new CPs, with formulas  $\{[\text{Ni}(\text{L1})(\text{nip})(\text{H}_2\text{O})]\cdot 2\text{H}_2\text{O}\}_n$  (**1**),  $[\text{Co}(\text{L2})(\text{tbip})]_n$  (**2**), and  $\{[\text{Co}_2(\text{L3})_2(\text{bptc})]\cdot 3\text{H}_2\text{O}\}_n$  (**3**) (L1 = 1,4-bis(5,6-dimethylbenzimidazole)butane, L2 = 1,4-bis(5,6-dimethylbenzimidazole)-2-butylene, L3 = 1,3-bis(5,6-dimethylbenzimidazole)propane), (Scheme 1) were hydrothermally synthesized and characterized by single-crystal X-ray diffraction. The solid-state fluorescence and catalytic properties of these complexes for the degradation of methyl orange in a Fenton-like process are described.

**Electronic supplementary material** The online version of this article (doi:10.1007/s11243-016-0045-4) contains supplementary material, which is available to authorized users.

✉ Gui Ying Dong  
tsdgying@126.com

<sup>1</sup> College of Chemical Engineering, North China University of Science and Technology, 46 West Xinhua Road, Tangshan 063009, Hebei, People's Republic of China

## Experimental

### Materials and methods

Reagents and solvents of analytical grade were obtained from commercial sources and used without further purification. The ligands L1, L2, and L3 were synthesized according to the literature procedures [21–23]. FTIR spectra (KBr pellets) were taken in the range of 4000–400  $\text{cm}^{-1}$  on an Avatar 360 (Nicolet) spectrophotometer. Elemental analyses were obtained on a PerkinElmer 240C Elemental Analyzer (C, H and N). Thermogravimetric analysis (TGA) was performed on a NETZSCH TG 209 thermal analyzer from room temperature to 800 °C with a heating rate of 10 °C/min under  $\text{N}_2$  atmosphere. Luminescence spectra were measured at room temperature on a Hitachi F-7000 fluorescence spectrophotometer. X-ray powder diffraction (XRPD) investigations were carried out with a Rigaku D/Max-2500PC X-ray diffractometer using  $\text{Cu-K}\alpha$  radiation ( $\lambda = 0.1542 \text{ nm}$ ) and  $\omega$ - $2\theta$  scan mode at 293 K (Scheme 1).

#### Synthesis of $\{[\text{Ni}(\text{L1})(\text{nip})(\text{H}_2\text{O})]\cdot 2\text{H}_2\text{O}\}_n$ (1)

A mixture of  $\text{Ni}(\text{OAc})_2\cdot 4\text{H}_2\text{O}$  (24.9 mg, 0.1 mmol), L1 (35.2 mg, 0.1 mmol),  $\text{H}_2\text{nip}$  (42.3 mg, 0.2 mmol), and  $\text{H}_2\text{O}$  (10 mL) was placed in a Teflon-lined stainless steel vessel (25 mL). The slurry was kept under magnetic stirring for 30 min at room temperature and then heated at 140 °C for 72 h. At the end of this period, the mixture was cooled to room temperature at a rate of 5 °C/h. Green block

single crystals of complex **1**, suitable for X-ray diffraction, were collected by filtration and washed with deionized water. Yield: 35 % (based on  $\text{Ni}(\text{OAc})_2\cdot 4\text{H}_2\text{O}$ ). Anal. Calcd. for  $\text{C}_{30}\text{H}_{35}\text{N}_5\text{NiO}_9$  (%): C, 53.9; H, 5.3; N, 10.5. Found (%): C, 54.1; H, 5.4; N, 10.4. IR (KBr,  $\text{cm}^{-1}$ ): 3430 (m), 3020 (m), 1680 (s), 1600 (m), 1570 (s), 1520 (s), 1470 (s), 1410 (m), 1350 (m), 1190 (w), 1140 (w), 910 (w), 729 (m), 554 (m), 478 (m), 421 (m).

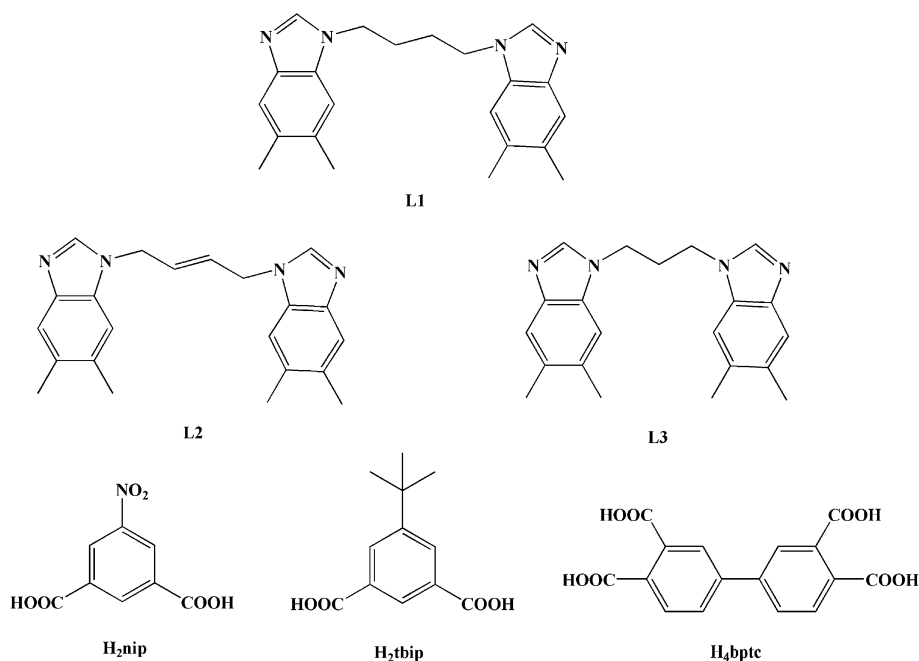
#### Synthesis of $[\text{Co}(\text{L2})(\text{tbip})]_n$ (2)

The synthesis method for complex **2** was similar to that of **1**, except that  $\text{Co}(\text{OAc})_2\cdot 4\text{H}_2\text{O}$  (25.0 mg, 0.1 mmol), L2 (69.3 mg, 0.2 mmol), and  $\text{H}_2\text{tbip}$  (54.2 mg, 0.2 mmol) were used instead of  $\text{Ni}(\text{OAc})_2\cdot 4\text{H}_2\text{O}$ , L1, and  $\text{H}_2\text{nip}$ . Red block single crystals of **2** were obtained with a yield of 45 % based on  $\text{Co}(\text{OAc})_2\cdot 4\text{H}_2\text{O}$ . Anal. Calcd. for  $\text{C}_{34}\text{H}_{36}\text{CoN}_4\text{O}_4$  (%): C, 65.5, H, 5.8, N, 9.0; Found (%): C, 65.7; H, 5.9; N, 9.1. IR (KBr,  $\text{cm}^{-1}$ ): 2960 (m), 2360 (w), 1620 (s), 1520 (s), 1450 (m), 1350 (s), 1210 (w), 987 (w), 843 (w), 782 (m), 725 (m), 625 (w).

#### Synthesis of $\{[\text{Co}_2(\text{L3})_2(\text{bptc})]\cdot 3\text{H}_2\text{O}\}_n$ (3)

The synthesis method for complex **3** was similar to that of **1**, except that  $\text{Co}(\text{OAc})_2\cdot 4\text{H}_2\text{O}$  (25.0 mg, 0.1 mmol), L3 (66.5 mg, 0.2 mmol), and  $\text{H}_4\text{bptc}$  (66.7 mg, 0.2 mmol) were used instead of  $\text{Ni}(\text{OAc})_2\cdot 4\text{H}_2\text{O}$ , L1, and  $\text{H}_2\text{nip}$ , respectively. Red block single crystals of **3** were obtained with a yield of 33 % based on  $\text{Co}(\text{OAc})_2\cdot 4\text{H}_2\text{O}$ . Anal. Calcd. for  $\text{C}_{58}\text{H}_{60}\text{Co}_2\text{N}_8\text{O}_{11}$  (%): C, 59.9; H, 5.2; N, 9.6;

**Scheme 1** Structural formulas of the L1, L2, L3, and organic acid ligands appeared in complexes 1–3



Found (%): C, 60.1; H, 5.3; N, 9.8. IR (KBr,  $\text{cm}^{-1}$ ): 3350 (m), 2940 (m), 2010 (w), 1660 (s), 1530 (s), 1420 (s), 1280 (m), 1160 (w), 1090 (w), 866 (m), 775 (m), 623 (w).

### X-ray crystallography

Crystallographic data for complexes **1** and **2** were collected on a Bruker Smart CCD diffractometer with Mo-K $\alpha$  radiation ( $\lambda = 0.71073 \text{ \AA}$ ) using an  $\omega$  scan mode, while crystallographic data for complex **3** were collected on an Agilent Technology SuperNova Atlas Dual System with Cu-K $\alpha$  radiation ( $\lambda = 1.54184 \text{ \AA}$ ) using an  $\omega$  scan mode. For complexes **1** and **2**, semiempirical absorption corrections were applied using the SADABS program [24], while the CrysAlis program [25] was used for complex **3**. All three structures were solved by direct methods and refined on  $F^2$  by full-matrix least-squares using the SHELXL-97 program package [26]. All nonhydrogen atoms were refined with anisotropic displacement parameters. Two water molecules in complex **1** and three water molecules in complex **3** were disordered, and their contribution to the scattering was taken into account by the application of the SQUEEZE routine of the PLATON program [27]. Crystal

parameters and details of the final refinement parameters are shown in Table 1. Selected bond lengths and angles for all three complexes are listed in Table 2.

### Catalysis experiments

Catalytic degradation of the dye was carried out in a 250-mL round-bottom flask, and the reaction temperature was controlled at 30 °C by circulating constant temperature water. A solution of methyl orange (150 mL with 10 mg/L) plus  $\text{Na}_2\text{S}_2\text{O}_8$  (30 mg) was placed in the flask. When the temperature was stabilized, the solid catalyst **1**, **2**, or **3** (50 mg) was added. At given time intervals, 5.0 mL aliquots of the suspension were collected and separated by centrifugation at 10,000 rpm for 15 min in order to remove catalyst particles. The supernatant was then analyzed using a UV-Vis 1910 spectrophotometer at  $\lambda = 506 \text{ nm}$ . The degradation efficiency was calculated as the percentage of discoloration according to Eq. (1) considering the initial and final absorbance values of the dye solution at a wavelength of 506 nm ( $A_0$  and  $A_t$ , respectively);

$$\text{Degradation efficiency} = (A_0 - A_t)/A_0 \times 100\% \quad (1)$$

**Table 1** Crystal and refinement data for complexes **1–3**

Complex	<b>1</b>	<b>2</b>	<b>3</b>
Chemical formula	$\text{C}_{30}\text{H}_{35}\text{N}_5\text{NiO}_9$	$\text{C}_{34}\text{H}_{36}\text{CoN}_4\text{O}_4$	$\text{C}_{58}\text{H}_{60}\text{Co}_2\text{N}_8\text{O}_{11}$
Formula weight	668.34	623.60	1163.03
Crystal system	Triclinic	Triclinic	Triclinic
Space group	$P\bar{1}$	$P\bar{1}$	$P\bar{1}$
$a$ ( $\text{\AA}$ )	9.513(4)	10.1756(8)	12.9362(6)
$b$ ( $\text{\AA}$ )	10.206(4)	10.1990(8)	14.4598(6)
$c$ ( $\text{\AA}$ )	17.749(8)	15.5806(8)	14.6661(5)
$\alpha$ ( $^\circ$ )	105.987(5)	87.801(5)	91.108(3)
$\beta$ ( $^\circ$ )	94.645(6)	76.999(6)	103.376(3)
$\gamma$ ( $^\circ$ )	107.192(5)	76.572(7)	94.711(4)
$V$ ( $\text{\AA}^3$ )	1557.6(12)	1532.29(19)	2657.85(19)
$Z$	2	2	2
$D_{\text{calcd}}$ ( $\text{g/cm}^3$ )	1.425	1.352	1.446
$\mu$ ( $\text{mm}^{-1}$ )	0.684	0.605	5.447
$F(000)$	700	654	1206
Total reflections	11,461	25,427	27,557
Unique reflections	5419	6264	9505
$R_{\text{int}}$	0.0414	0.0555	0.0774
GOF on $F^2$	1.078	1.048	1.101
$R_1$ ( $I > 2\sigma(I)$ )	0.1108	0.0499	0.0638
w $R_2$ ( $I > 2\sigma(I)$ )	0.3224	0.1180	0.1575
$\Delta\rho_{\text{max}}$ ( $\text{e}\text{\AA}^{-3}$ )	1.925	1.031	0.699
$\Delta\rho_{\text{min}}$ ( $\text{e}\text{\AA}^{-3}$ )	-1.117	-0.447	-0.657

**Table 2** Selected bond lengths [Å] and angles [°] for complexes **1–3**

Parameter	Value	Parameter	Value
<b>1</b>			
Ni(1)–O(3)	2.017(7)	Ni(1)–O(1 W)	2.075(8)
Ni(1)–N(4)	2.080(8)	Ni(1)–N(2)A	2.096(8)
Ni(1)–O(5)B	2.115(6)	Ni(1)–O(6)B	2.147(7)
O(3)–Ni(1)–O(1 W)	96.2(3)	O(3)–Ni(1)–N(4)	87.5(3)
O(1 W)–Ni(1)–N(4)	90.8(3)	O(3)–Ni(1)–N(2)A	90.4(3)
O(1 W)–Ni(1)–N(2)A	92.6(3)	N(4)–Ni(1)–N(2)A	176.2(3)
O(3)–Ni(1)–O(5)B	166.0(3)	O(1 W)–Ni(1)–O(5)B	97.8(3)
N(4)–Ni(1)–O(5)B	92.0(3)	N(2)A–Ni(1)–O(5)B	89.2(3)
O(3)–Ni(1)–O(6)B	103.8(3)	O(1 W)–Ni(1)–O(6)B	159.9(3)
N(4)–Ni(1)–O(6)B	91.4(3)	N(2)A–Ni(1)–O(6)B	86.1(3)
O(5)B–Ni(1)–O(6)B	62.2(3)		
<b>2</b>			
Co(1)–O(1)A	2.0008(19)	Co(1)–O(3)	2.009(2)
Co(1)–N(3)	2.024(2)	Co(1)–N(1)	2.049(3)
Co(1)–O(2)A	2.397(2)		
O(1)A–Co(1)–O(3)	100.16(8)	O(1)A–Co(1)–N(3)	117.73(9)
O(3)–Co(1)–N(3)	100.05(9)	O(1)A–Co(1)–N(1)	113.10(9)
O(3)–Co(1)–N(1)	100.18(9)	O(3)–Co(1)–N(1)	120.07(10)
O(1)A–Co(1)–O(2)A	59.49(7)	O(3)–Co(1)–O(2)A	159.39(8)
N(3)–Co(1)–O(2)A	88.13(8)	N(1)–Co(1)–O(2)A	91.78(8)
<b>3</b>			
Co(1)–O(2)	1.958(3)	Co(1)–O(3)A	1.965(3)
Co(1)–N(1)B	2.042(4)	Co(1)–N(8)	2.042(4)
Co(2)–O(5)C	1.944(3)	Co(2)–O(8)D	1.950(3)
Co(2)–N(5)	2.020(4)	Co(2)–N(4)	2.034(4)
O(2)–Co(1)–O(3)A	130.60(14)	O(2)–Co(1)–N(1)B	92.61(14)
O(3)A–Co(1)–N(1)B	104.18(14)	O(2)–Co(1)–N(8)	119.91(14)
O(3)A–Co(1)–N(8)	98.91(14)	N(1)B–Co(1)–N(8)	107.59(15)
O(5)C–Co(2)–O(8)D	110.08(13)	O(5)C–Co(2)–N(5)	105.11(14)
O(8)D–Co(2)–N(5)	123.55(15)	O(5)C–Co(2)–N(4)	120.69(14)
O(8)D–Co(2)–N(4)	93.79(14)	N(5)–Co(2)–N(4)	104.51(15)

Symmetry codes for **1**: A:  $x + 1, y + 1, z$ , B:  $x, y + 1, z$ , for **2**: A:  $x, y + 1, z$ , for **3**: A:  $-x + 1, -y + 1, -z + 2$ , B:  $-x + 2, -y + 1, -z + 2$ , C:  $x + 1, y, z$ , D:  $-x + 1, -y, -z + 1$

## Results and discussion

### Crystal structure of complex **1**

Structure analysis shows that complex **1** crystallizes in the triclinic space group  $P\bar{1}$ . The asymmetric unit contains one Ni(II) center, one L1 ligand, one  $\text{nip}^{2-}$  anion, and one water ligand, plus two lattice water molecules (squeezed). The coordination environment of the Ni center is shown in Fig. 1a. Each Ni(II) center is six-coordinated by two nitrogen atoms (Ni1–N2A = 2.096(8) Å, Ni1–N4 = 2.080(8) Å, symmetry code: A =  $x + 1, y + 1, z$ ) from two different L1 ligands, three oxygen atoms (Ni1–O3 = 2.017(7) Å, Ni1–O5B = 2.115(6) Å, Ni1–O6B =

2.147(7) Å) from the carboxylate groups of two distinct  $\text{nip}^{2-}$  anions, and one O atom from a coordinated water ligand (Ni1–O1 W = 2.075(8) Å), completing the distorted octahedral geometry. The coordination angles range from 62.2(3)° to 176.2(3)°, which are similar to those in other nickel coordination complexes [28].

In complex **1**, the completely deprotonated  $\text{nip}^{2-}$  anions adopt the  $\mu_2\text{-}\eta^2\text{:}\eta^1$  coordination mode, connecting neighboring Ni atoms to construct a 1D linear chain along the  $b$ -axis with a nonbonding Ni···Ni distance of 10.206(4) Å. The adjacent 1D chains are further connected by the L1 ligands in a  $\mu_2$ -bridging mode to construct a 2D sheet (Fig. 1b), in which the 38-membered parallelogram units consist of four Ni atoms at the corners connected by two L1

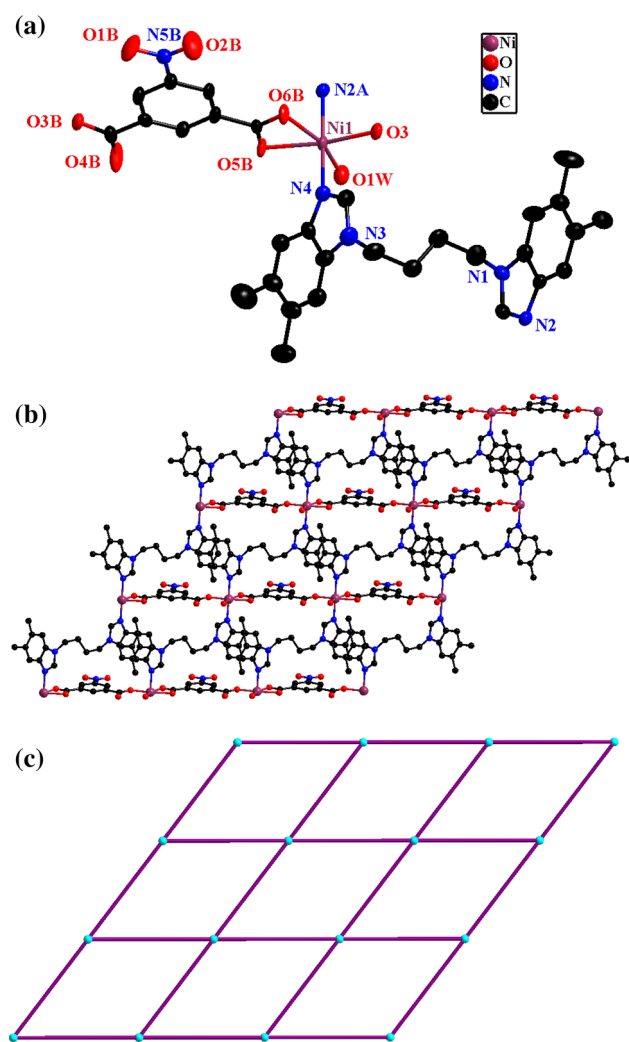


**Fig. 1** **a** Coordination environment of Ni atom in **1**. Hydrogen atoms are omitted for clarity (30 % ellipsoid probability). Symmetry codes: A:  $x + 1, y + 1, z$ , B:  $x, y + 1, z$ . **b** Ball-and-stick view of the 2D network structure in **1**. **c** sql topology network of **1**

and two nip ligands. Meanwhile, the L1 ligand acting in an *anti*-conformation connects two Ni atoms with a non-bonding Ni...Ni separation of 11.716(4) Å, the dihedral angle between its benzimidazole rings of 4.381(3)°. From a topological viewpoint, the structure of **1** can be simplified to uninodal 2D (4,4)-network of **sql** topology with a point symbol of ( $4^4 \times 6^2$ ) (Fig. 1c), in which the dimensions are 10.206(4) Å  $\times$  11.716(4) Å defined by Ni...Ni separations.

### Crystal structure of complex **2**

Structure analysis reveals that complex **2** has a 2D wave-like network, crystallizing in the triclinic system  $P\bar{1}$  space group. The asymmetric unit consists of one independent Co(II) center, two halves of L2 ligands, and one  $\text{tbip}^{2-}$  anion (Fig. 2a). The Co(II) center displays a five-

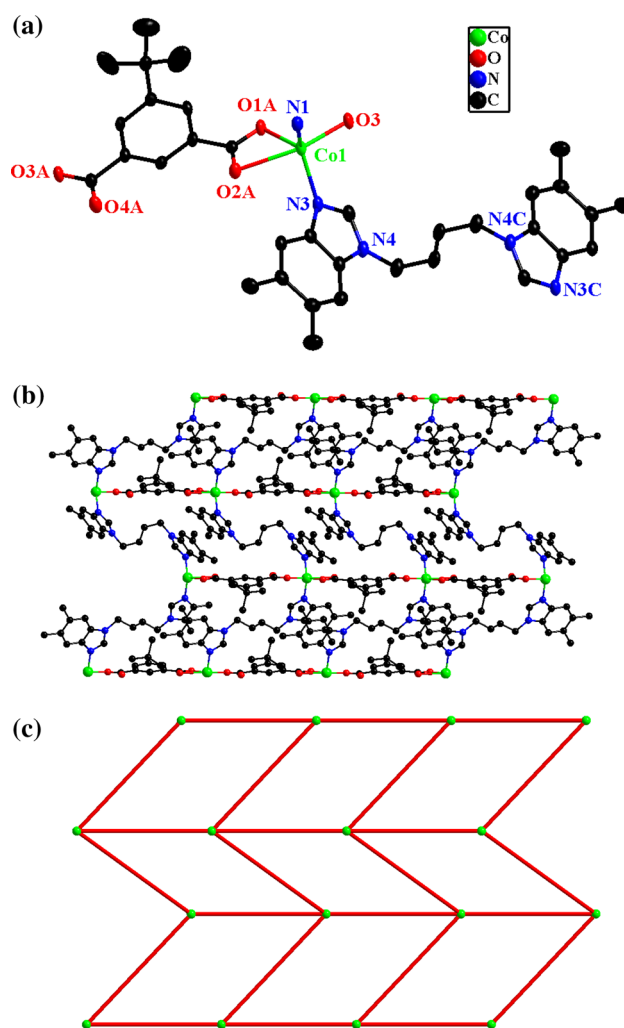


**Fig. 2** **a** Coordination environment of Co atom in **2**. Hydrogen atoms are omitted for clarity (30 % ellipsoid probability). Symmetry codes: A:  $x, y + 1, z$ , C:  $-x + 1, -y + 1, -z + 1$ . **b** Ball-and-stick view of the 2D network structure in **2**. **c** sql topology network of **2**

coordinated mode, provided by three O atoms from two  $\text{H}_2\text{tbip}$  carboxyl groups (Co1–O1A = 2.001(2) Å, Co1–O2A = 2.397(2) Å, Co1–O3 = 2.009(2) Å, symmetry code: A =  $x, y + 1, z$ ) and two N atoms from two L2 ligands (Co1–N1 = 2.049(3) Å, Co1–N3 = 2.024(2) Å), resulting in a distorted trigonal bipyramidal geometry. The N–Co–O bond angles are in the range from 88.13(8)° to 117.73(9)°, while the O–Co–O bond angles vary from 59.49(7)° to 159.39(8)°.

The ligand L2 has a bis-monodentate bridging coordination mode. The nitrogen atoms from two benzimidazole rings of L2 connect adjacent Co atoms to form an infinite  $\Omega$   $[\text{Co}(\text{L}2)]_n$  chain in which the distances between Co centers are 11.504(1) and 11.852(1) Å, and the two benzimidazole rings of the L2 ligands are parallel to each other. The  $\text{tbip}^{2-}$  anion exhibits two kinds of coordination mode,

specifically monodentate and bidentate. The oxygen atoms of tbip ligands bridge neighboring Co(II) atoms to build an infinite straight chain, in which the Co–Co distance is 10.199(2) Å. The two 1D chains are cross-linked to compose a 2D wavelike network (Fig. 2b), whose dimensions are 10.199(1) Å × 11.852(11) Å defined by Co...Co separations. In this complex, the Co atom can be simplified as a 4-connected node, while the two organic ligands are considered to be linear linkers. As a result, the 2D network can be best described as a (4,4)-connected network with a point symbol of (4<sup>4</sup> × 6<sup>2</sup>) (Fig. 3b).

### Crystal structure of complex 3

Complex 3 crystallizes in the triclinic crystal system with *P*1 space group. The asymmetric unit consists of two Co(II) centers, two L3 ligands, one bptc<sup>4-</sup> anion, and three lattice water molecules (squeezed). The two independent Co(II) centers both display a distorted tetrahedral coordination geometry. As shown in Fig. 3a, the Co1 center is four-coordinated by two O atoms (O2, O3A, symmetry code: A = -x + 1, -y + 1, -z + 2) from two bptc<sup>4-</sup> anions and two N atoms (N1B, N8, symmetry code: B = -x + 2, -y + 1, -z + 2) from two L3 ligands. The Co–N bond

distances for Co1 are 2.042(4) Å, and the Co–O lengths are 1.958(3) and 1.965(3) Å; these values are in good agreement with those of similar Co(II) complexes [29]. The coordination environment of Co2 is similar to that of Co1, the Co2 atom coordinated by two N atoms (N4, N5) from different L3 ligands with bond distances of 2.020(4) and 2.034(4) Å, plus two O atoms (O5C, O8D, symmetry code: C = x + 1, y, z, D = -x + 1, -y, -z + 1) from different bptc<sup>4-</sup> anions with bond distances of 1.944(3) and 1.950(3) Å.

In complex 3, the bptc<sup>4-</sup> anion, which is fully deprotonated, adopts a  $\mu_4-\eta^1:\eta^1:\eta^1:\eta^1$  coordination mode. The four-connected bptc<sup>4-</sup> anions link adjacent cobalt atoms (Co1 and Co2) to construct a 1D wavelike chain, which is further extended into a 2D network (Fig. 3b) via the bridging L3 ligands. The L3 ligands exhibit a *cis*-conformation mode with dihedral angles between the benzimidazole rings of 57.990(2)° and 55.900(2)°. Four L3 ligands connect adjacent cobalt atoms to generate a 40-membered macrocycle (Fig. 3c), in which the four Co atoms act as nodes with dimensions of 12.791 × 17.852 Å.

As discussed above, each Co atom is linked by two bptc<sup>4-</sup> anions and two L3 ligands, which can be defined as a 4-connected node. Each deprotonated bptc<sup>4-</sup> ligand links

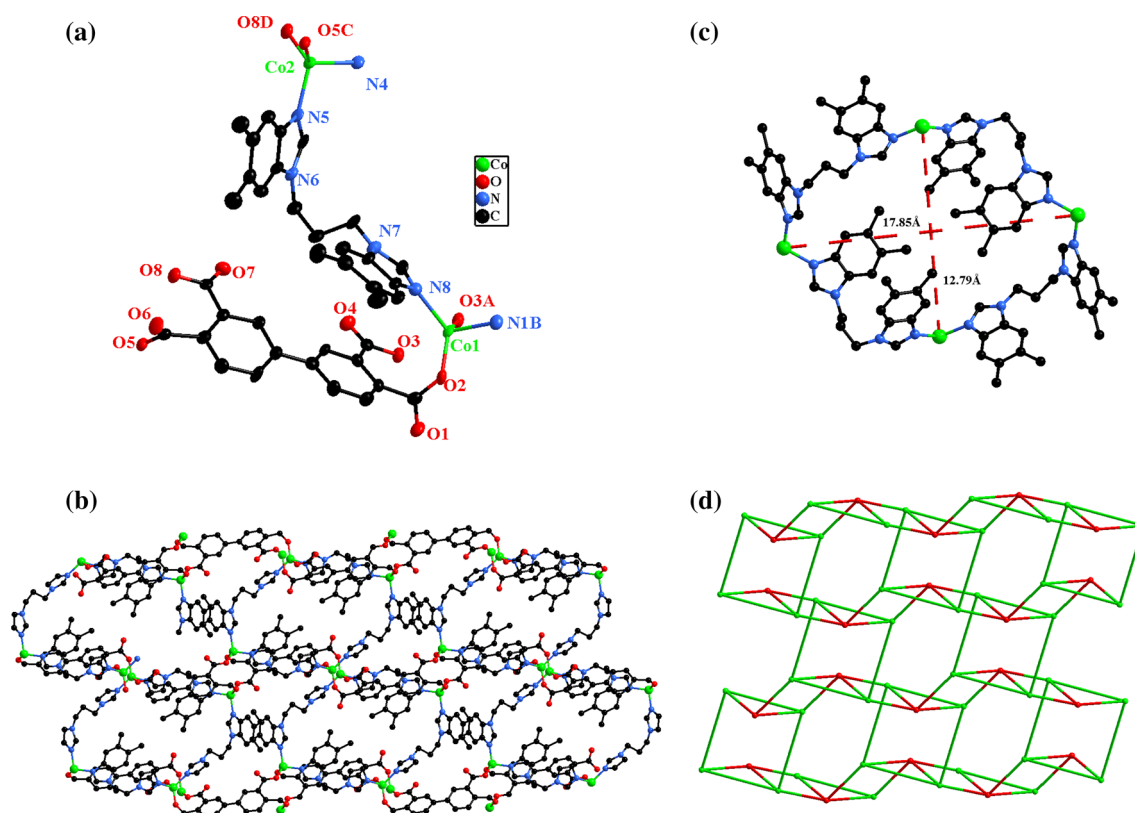


**Fig. 3** **a** Coordination environment of Co atom in 3. Hydrogen atoms are omitted for clarity (30 % ellipsoid probability). Symmetry codes: A: -x + 1, -y + 1, -z + 2, B: -x + 2, -y + 1, -z + 2, C: x + 1,

y, z, D: -x + 1, -y, -z + 1. **b** Ball-and-stick view of the 2D network structure in 3. **c** Macrocycle generated by L3 ligands. **d** htb topology network of 3

four Co atoms, which can be simplified as a 4-connected node, and the L3 ligands can be viewed as linkers. Thus, the uninodal **htb** (hexagonal tungsten bronzes) [30] topology was obtained with a point symbol of  $(3.4^2 \times 5^2.6)$  (Fig. 3d).

### Influence of organic ligands on the structures

In similar hydrothermal reactions, three flexible bis(5,6-dimethylbenzimidazole) ligands and three aromatic carboxylic acids were assembled with Ni(II) and Co(II) atoms, yielding complexes with diverse structures. In each case, the flexible bis(5,6-dimethylbenzimidazole) derivatives adopt a bis-monodentate bridging coordination mode to link the Ni or Co atoms, but these ligands exhibit different bending and rotating abilities, leading to different distances between the metal centers (11.716(4) Å for **1**, 11.504(1) and 11.852(1) Å for **2**, 10.321(1) and 10.630(1) Å for **3**) and distinct dihedral angles between the mean planes of the benzimidazole rings ( $4.381(3)^\circ$  for **1**,  $0^\circ$  for **2**,  $57.990(2)^\circ$  and  $55.900(2)^\circ$  for **3**). The  $\text{nip}^{2-}$  anions in **1** and the  $\text{tbip}^{2-}$  anions in **2** both display the  $\mu_2\text{-}\eta^2\text{:}\eta^1$  coordination mode, connecting adjacent metal atoms to give infinite 1D chains. In complex **3**, the  $\text{bptc}^{4-}$  anions adopt a  $\mu_4\text{-}\eta^1\text{:}\eta^1\text{:}\eta^1\text{:}\eta^1$  coordination mode, in which the four-connected  $\text{bptc}^{4-}$  anions link neighboring cobalt atoms (Co1 and Co2) to construct a 1D wavelike chain. Finally, the combination of carboxylate and N-containing co-ligands leads to the construction of two different topological networks: uninodal 2D (4,4)-network of **sql** topology for complexes **1** and **2**, and uninodal 2D 4-connected **htb** topology framework for complex **3**.

### IR and X-ray powder diffraction studies

Figure S1 presents the IR spectra of complexes **1–3** in the range of  $4000\text{--}400\text{ cm}^{-1}$ . In these spectra, the  $\nu_{(\text{C}=\text{N})}$  breathing vibrations of the benzimidazole rings are observed at  $1570$ ,  $1520$ , and  $1530\text{ cm}^{-1}$ , respectively [31]. There is no absorption around  $1700\text{ cm}^{-1}$  for any of these complexes, indicating that all carboxylic acid groups are fully deprotonated [32]. For complex **1**, a strong broad band at around  $3400\text{ cm}^{-1}$  can be assigned to the O–H stretching vibrations of water molecules or hydrogen bonds. The IR spectrum of complex **1** also shows the carboxylic group at  $1680\text{ cm}^{-1}$  for the antisymmetric stretching and  $1520$  plus  $1470\text{ cm}^{-1}$  for the symmetric stretching modes. The separations of  $\nu_{\text{as}}$  and  $\nu_{\text{s}}$  ( $\Delta\nu = 160\text{ cm}^{-1}$  and  $210\text{ cm}^{-1}$ ) imply the presence of both chelating and monodentate carboxylic groups [33]. For complex **2**, the strong characteristic band of the carboxylic groups appears at  $1620\text{ cm}^{-1}$  for the antisymmetric stretching and  $1520$  plus  $1350\text{ cm}^{-1}$  for the symmetric

stretching modes, indicating the presence of both chelating and monodentate ( $\Delta\nu = 100\text{ cm}^{-1}$  and  $270\text{ cm}^{-1}$ ) carboxylic groups. In complex **3**, absorptions at ca.  $3350\text{ cm}^{-1}$  are assigned to the stretching vibrations of free water molecules. The antisymmetric and symmetric stretching vibrations of the carboxylic groups are observed at  $1660$  and  $1420\text{ cm}^{-1}$ , respectively, confirming that the carboxylic groups of complex **3** adopt a monodentate bridging mode with  $\Delta\nu = 240\text{ cm}^{-1}$ .

The experimental and computer-simulated X-ray powder diffraction (XRPD) patterns of complexes **1–3** are shown in Fig. S2. There is good agreement between the patterns, indicating that the bulk samples have the same structures as the crystals. The different intensities may be derived from the variation in preferred orientations of the powder samples during the collection of data [34].

### Thermal and fluorescent properties

Thermogravimetric experiments (TGA) were carried out for complexes **1–3** under nitrogen atmosphere to investigate their thermal stabilities, with the results shown in Fig. 4. Complexes **1** and **3** both gave a two-step weight loss process. The first process of complex **1** occurs from  $100$  to  $180^\circ\text{C}$  with a weight loss of  $8.1\%$ , which can be attributed to the loss of water molecules (calcd:  $8.2\%$ ). The second weight loss is assigned to decomposition of the organic ligands in the region of  $290\text{--}630^\circ\text{C}$ . The residual weight  $11.9\%$  (calcd:  $12.0\%$ ) corresponds to NiO. In complex **2**, the single weight loss of  $87.9\%$  (calcd:  $87.8\%$ ) from  $320$  to  $630^\circ\text{C}$  is attributed to decomposition of the L2 and  $\text{H}_2\text{tbip}$  ligands, resulting in the formation of CoO. The TGA curve of complex **3** shows the loss of lattice water molecules with  $4.6\%$  (calcd:  $4.6\%$ ), which begins at  $30^\circ\text{C}$  and is complete by  $203^\circ\text{C}$ . The residue is

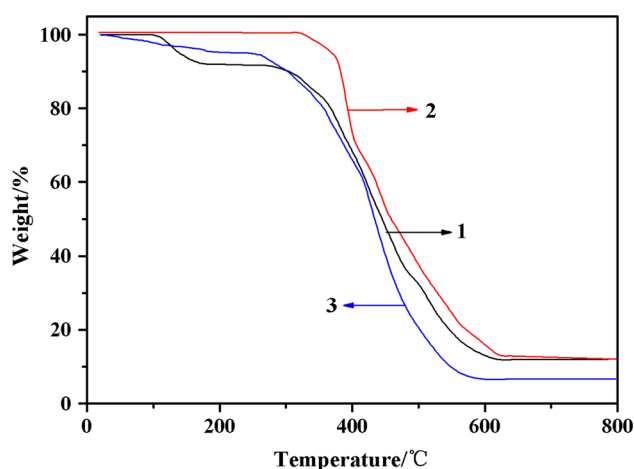


**Fig. 4** TGA curves of polymers **1–3** were measured in  $\text{N}_2$  atmosphere

stable up to 240 °C and then loses the weight of L3 and H<sub>4</sub>bptc ligands until up 600 °C. Finally, a CoO remnant of 6.4 % (calcd. 6.5 %) is obtained.

The solid-state fluorescence properties of the free ligands L1–L3 as well as complexes **1**–**3** have been investigated at room temperature. As shown in Fig. 5, the free ligands display strong emission maxima at 369, 359, and 349 nm upon excitation at 320, 280, and 310 nm for L1, L2, and L3, respectively, which may be attributed to  $\pi^* \rightarrow n$  or  $\pi^* \rightarrow \pi$  transitions [35]. For the complexes, the emission maxima are at 394 nm ( $\lambda_{\text{ex}} = 250$  nm), 325 nm ( $\lambda_{\text{ex}} = 320$  nm), and 396 nm ( $\lambda_{\text{ex}} = 275$  nm) for **1**, **2**, and **3**, respectively. Compared with the free ligands L1 and L2, the maxima of complexes **1** and **3** are red-shifted, which may be attributed to intraligand charge transfer transitions [36]. However, a blue-shifted emission is observed for complex **2** with respect to free L2, which can be tentatively assigned to ligand-to-metal charge transfer transitions [37].

### Catalytic properties

Methyl orange (MO) is a well-known azo dye that has been used for textiles, printing, paper, rubber, plastic, and research [38, 39]. However, it is also potentially harmful to the environment because of its high chemical stability and low biodegradability [40]. Therefore, MO was selected as a model organic pollutant to study the catalytic behavior of complexes **1**–**3**. An oxidation technology based on strongly oxidizing sulfate radicals ( $\text{SO}_4^{\cdot-}$ ) has recently been developed for the degradation of organic pollutants resistant to conventional technologies [41]. Thus, persulfate anions can be converted into sulfate radicals ( $\text{SO}_4^{\cdot-}$ ), which are effective oxidants for organic pollutants. Here, complexes

**1**–**3** were tested as heterogeneous catalysts for the activation of  $\text{Na}_2\text{S}_2\text{O}_8$ .

The results of these MO degradation experiments are shown in Fig. 6. In a control experiment (without added catalyst), the azo dye and  $\text{Na}_2\text{S}_2\text{O}_8$  mixture showed only 19.4 % degradation of MO after 120 min. Upon addition of complexes **1**–**3** as heterogeneous catalysts, degradation efficiencies increased to 73 % for complex **1**, 70 % for complex **2**, and 61 % for complex **3** after 120 min. Nevertheless, the catalytic efficiencies of these complexes are lower than those of other Ni(II) and Co(II) complexes reported in the literature [42, 43].

### Conclusion

In conclusion, three new coordination polymers based on flexible bis(5,6-dimethylbenzimidazole) ligands and aromatic carboxylate co-ligands have been synthesized and characterized. The variable coordination modes of the carboxylate ligands play an essential role in the construction of these CPs, while the flexible bis(5,6-dimethylbenzimidazole) ligands display the ability to adjust their conformations to meet the coordination requirements of the metal centers. Complexes **1**–**3** show moderate catalytic activities in the Fenton-like decomposition of methyl orange.

### Supplementary materials

CCDC depository numbers 1421229 for **1**, 1447780 for **2**, and 1446477 for **3** contain the supplementary crystallographic data for the complexes **1**–**3**. These data can be obtained free of charge via <https://www.ccdc.cam.ac.uk/>,

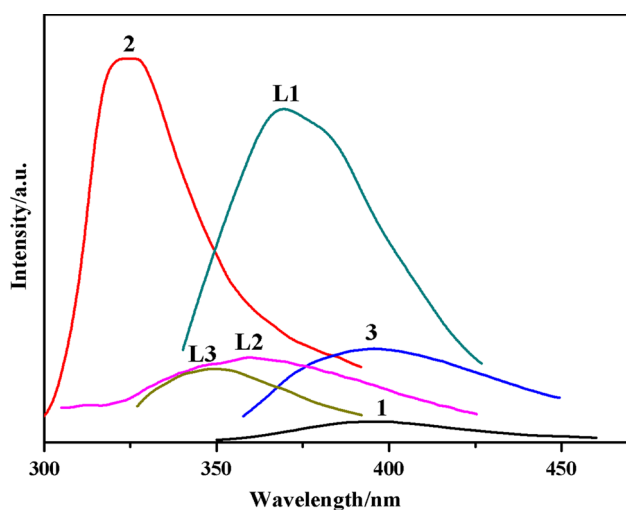


Fig. 5 Emission spectra of complexes **1**–**3** and the free ligands

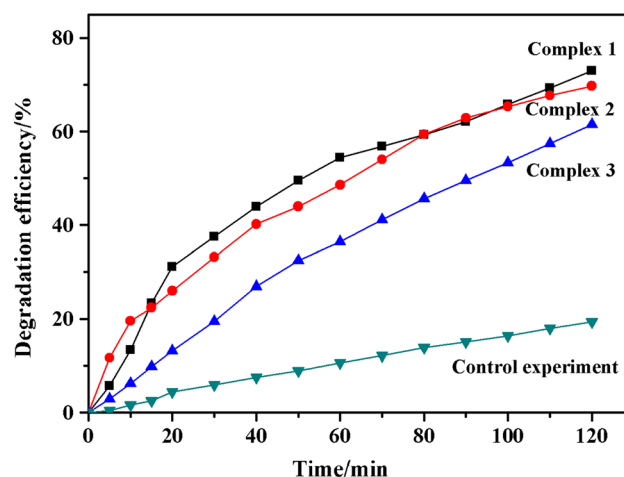


Fig. 6 Experiment results of the catalytic degradation of methyl orange azo dye

or from the Cambridge Crystallographic Data Centre, 12 Union Road, Cambridge CB2 1EZ, UK; fax: (+44) 1223-336-033; or e-mail: deposit@ccdc.cam.ac.uk.

**Acknowledgments** The project was supported by the National Natural Science Foundation of China (51474086), Natural Science Foundation-Steel and Iron Foundation of Hebei Province (B2015209299).

## References

1. Dhakshinamoorthy A, Garcia H (2014) *Chem Soc Rev* 43:5750–5765
2. Morris RE, Wheatley PS (2008) *Angew Chem Int Ed* 47:4966–4981
3. Wang XX, Ma YJ, Li HH, Cui GH (2015) *Transit Met Chem* 40:99–108
4. Maji TK, Uemura K, Chang HC, Matsuda R, Kitagawa S (2004) *Angew Chem Int Ed* 116:3331–3334
5. Cui GH, He CH, Jiao CH, Geng JC, Blatov VA (2012) *CrystEngComm* 14:4210–4216
6. Qin JH, Ma LF, Hu Y, Wang LY (2012) *CrystEngComm* 14:2891–2898
7. Hu JM, Blatov VA, Yu B, Hecke KV, Cui GH (2016) *Dalton Trans* 45:2426–2429
8. Yang GP, Wang YY, Ma LF, Liu JQ, Wu YP, Wu WP, Shi QZ (2007) *Eur J Inorg Chem* 2007:3892–3898
9. Wang XL, Chen YQ, Liu GC, Zhang JX, Lin HY, Chen BK (2010) *Inorg Chim Acta* 363:773–778
10. Hao JM, Yu BY, Van Hecke K, Cui GH (2015) *CrystEngComm* 17:2279–2293
11. Zhu X, Wang N, Luo Y, Pang Y, Tian D, Zhang H (2011) *Aust J Chem* 64:1346–1354
12. Sun R, Li YZ, Bai J, Pan Y (2007) *Cryst Growth Des* 7:890–894
13. Hsu YF, Hsu W, Wu CJ, Cheng PC, Yeh CW, Chang WJ, Chen JD, Wang JC (2010) *CrystEngComm* 12:702–710
14. Ma LF, Wang LY, Lu DH, Batten SR, Wang JG (2009) *Cryst Growth Des* 9:1741–1749
15. Wang JJ, Gou L, Hu HM, Han ZX, Li DS, Xue GL, Yang ML, Shi QZ (2007) *Cryst Growth Des* 7:1514–1521
16. Zhang X, Dong GY, Yu B, Van Hecke K, Cui GH (2015) *Transit Met Chem* 40:907–916
17. Wang XX, Liu YG, Ge M, Cui GH (2015) *Chin J Inorg Chem* 31:2065–2072
18. Wang XL, Sui FF, Lin HY, Zhang JW, Liu GC (2014) *Cryst Growth Des* 14:3438–3452
19. Xiao SL, Li YH, Ma PJ, Cui GH (2013) *Inorg Chem Commun* 37:54–58
20. Qin L, Li YH, Ma PJ, Cui GH (2013) *J Mol Struct* 1051:215–220
21. Li LL, Li HX, Ren ZG, Liu D, Chen Y, Zhang Y, Lang JP (2009) *Dalton Trans* 8567–8573
22. Geng JC, Qin L, Du X, Xiao SL, Cui GH (2012) *Z Anorg Allg Chem* 638:1233–1238
23. Liu GC, Yang S, Wang XL, Lin HY, Tian AX, Zhang JW (2012) *Koord Khim* 38:55–60
24. Sheldrick GM (1996) SADABS. University of Göttingen, Germany
25. Agilent Technologies (2012) CrysAlis PRO Agilent technologies. Yarnton, England
26. Sheldrick GM (2007) *Acta Cryst A* 64:112–122
27. Spek AL (2009) *Acta Cryst D* 65:148–155
28. Liu XB, Huang CM, Dong GY, Cui GH (2015) *Transit Met Chem* 40:847–856
29. Chen N, Yang P, He X, Shao M, Li MX (2013) *Inorg Chim Acta* 405:43–50
30. Magneli A (1953) *Acta Chem Scand* 7:315–324
31. Geng JC, Qin L, He CH, Cui GH (2012) *Transit Met Chem* 37:579–585
32. Liu GC, Huang JJ, Zhang JW, Wang XL, Lin HY (2013) *Transit Met Chem* 38:359–365
33. Deacon G, Phillips R (1980) *Coord Chem Rev* 33:227–250
34. Zhao HY, Zhao JW, Yang BF, He H, Yang GY (2013) *Cryst Growth Des* 13:5169–5174
35. Huang XY, Yue KF, Jin JC, Liu JQ, Wang CJ, Wang YY, Shi QZ (2010) *Inorg Chem Commun* 13:338–341
36. Zhang MD, Qin L, Yang HT, Li YZ, Guo ZJ, Zheng HG (2013) *Cryst Growth Des* 13:1961–1969
37. Huang XJ, Xia Y, Zhang HR, Yan ZZ, Tang Y, Yang XJ, Wu B (2008) *Inorg Chem Commun* 11:450–453
38. Purkait MK, Vijay SS, Dasgupta S, De S (2004) *Dyes Pigm* 63:151–159
39. Ma LF, Meng QL, Li CP, Li B, Wang LY, Du M, Liang FP (2010) *Cryst Growth Des* 10:3036–3043
40. Mane VS, Babu PV (2013) *J Taiwan Inst Chem Eng* 44:81–88
41. Hussain I, Zhang Y, Huang S, Du X (2012) *Biochem Eng J* 203:269–276
42. Hu JM, Zhao YQ, Baoyi Y, Van Hecke K, Cui GH (2016) *Z Anorg Allg Chem* 624:41–47
43. Wang XX, Zhang S, Van Hecke K, Cui GH, Liu YG (2015) *Transit Met Chem* 40:565–571